# **Enhanced Reverse Intersystem Crossing**

## **Promoted by Triplet Exciton-Photon Coupling**

Qi Ou ,† Yihan Shao,‡ and Zhigang Shuai\*,†

†MOE Key Laboratory of Organic OptoElectronics and Molecular Engineering, Department of Chemistry, Tsinghua University, Beijing 100084, China.

‡Department of Chemistry and Biochemistry, University of Oklahoma, Norman, Oklahoma
73019, USA

E-mail: zgshuai@tsinghua.edu.cn

#### Abstract

Polaritons are hybrid light-matter states formed via strong coupling between excitons and photons inside a microcavity, leading to upper and lower polariton (LP) bands splitting from the exciton. The LP has been applied to reduce the energy barrier of the reverse intersystem crossing (rISC) process from  $T_1$ , harvesting triplet energy for fluorescence through thermally activated delayed fluorescence. The spin-orbit coupling between  $T_1$  and excitonic part of LP was considered as the origin for such rISC transition. Here we propose a mechanism, namely, the rISC promoted by the light-matter coupling (LMC) between  $T_1$  and the cavity photonic mode, which is originated from the ISC-inducedtransition dipole moment of  $T_1$ . This mechanism was excluded in previous studies. Our calculations demonstrate that the experimentally observed enhancement to the rISC process of Erythrosine B molecule can be effectively promoted by the LMC between  $T_1$  and photon. The proposed mechanism would substantially broaden the aperture of the molecular design towards highly efficient cavity-promoted light-emitting materials and immediately benefit the illumination of related experimental phenomena.

#### Introduction

In organic microcavities, molecular excitons may strongly couple to the quantized radiation field, forming hybridized light-matter states which are known as exciton polaritons. <sup>1–5</sup> Over the past few decades, exciton polaritons have been extensively investigated both experimentally and theoretically, offering a vast number of potential applications in the field of physical and chemical sciences such as manipulating chemical reactivities, <sup>6–9</sup> promoting remote energy transfer, <sup>10–13</sup> modifying the rate constants of electronic relaxation, <sup>7,14,15</sup> and realizing polaritonic lasers. <sup>16–19</sup> One of the interesting applications of exciton polaritons is the enhancement to the reverse intersystem crossing (rISC) process of thermally activated delayed fluorescence (TADF) materials, which could further increase the exciton utilization efficiency under current injection and thus would be strongly favored in organic light-emitting devices. <sup>20–23</sup>

While multiple studies have reported the polariton-enhanced rISC process within organic molecules,  $^{15,24-26}$  whether such enhancement is indeed effective remains an open question. As pointed out by Yuen-Zhou and co-workers, at light-matter resonance, the rISC rate constant from triplet to the polariton state is inversely proportional to the number of molecules coupling with the photon (denoted as  $N_{\rm eff}$ ), given that the polariton is delocalized across  $N_{\rm eff}$  singlets and only one of them can undergo coupling to a given triplet.  $^{27,28}$  Therefore, organic microcavity systems, of which the number of coupled molecules can be as large as  $10^5$  to  $10^6$ , can hardly obtain an enhanced rISC process unless (i) the singlet-triplet mixing of the emitter is weak and (ii) the transition between triplet and singlet exciton is within the inverted Marcus regime, as theoretically demonstrated via a quantum mechanical model in Ref. 27. A direct calculation of the experimental observed polariton-enhanced rISC rate constant of realistic systems is, however, yet to be performed to essentially resolve the ambiguity. Accurate prediction on the rISC rate constant is a long-standing challenge for theoretical chemistry since it spans a wide time scale depending on the target systems, and can be significantly longer than the typical time span of the best-available excited state

dynamics simulation nowadays.  $^{29-31}$  Rate formalism such as the thermal vibration correlation function (TVCF) theory has become the practical approach to quantitatively describe the ISC/rISC process.  $^{32-34}$ 

In this work, focusing on one of the reported systems with polariton-enhanced rISC phenomenon, i.e., Erythrosine B (ErB) molecule (see Figure S1 for its chemical structure), <sup>15</sup> we apply properly benchmarked electronic structure theory and TVCF rate formalism to quantify its rISC enhancement inside the cavity. Most importantly, while the spin-orbit coupling (SOC) between triplets and singlets and/or polaritons has been considered as the only promoting force for rISC, we propose that the light-matter coupling (LMC) between T<sub>1</sub> and the cavity mode can be another promoting force that initiates rISC inside the cavity for molecules with non-negligible transition dipole moment (TDM) of T<sub>1</sub> such as ErB. The good agreement between our computational results and the previous experimental data rationalizes our theoretical protocol and demonstrates that the enhancement to the rISC of ErB inside the cavity can be effectively promoted by the LMC between T<sub>1</sub> and the photon. The proposed mechanism on polariton-enhanced rISC process can be immediately applied to vindicate related experimental observations as well as enlighten the design of organic microcavities with efficient TADF phenomena.

## Theory

For N identical molecules that lie inside an optical cavity, in the strong coupling regime, the coupling strength of the i<sup>th</sup> molecule to the vacuum electromagnetic field is <sup>4</sup>

$$\hbar g_i = \|\boldsymbol{\mu}\| \sqrt{\frac{\hbar \omega_c}{2\epsilon_0 \epsilon_\infty V}} \cos \theta_i \tag{1}$$

where  $\mu$  is the TDM of the S<sub>1</sub> state;  $\omega_c$  is the frequency of the cavity mode;  $\epsilon_0$  is the vacuum permitivity;  $\epsilon_{\infty}$  is the optical dielectric constant of the matrix inside the cavity; V is the cavity mode volume; and  $\theta_i$  is the angle between the TDM of the  $i^{\text{th}}$  S<sub>1</sub> and the

electromagnetic field. Note that if  $\theta_i = 90^{\circ}$ , the S<sub>1</sub> state of the  $i^{\text{th}}$  molecule will not effectively couple to the field.

Supposing the excitonic coupling among the  $S_1$  states of these N molecules is insignificant, we would have one lower polariton (LP) state and one upper polariton (UP) state, as well as N-1 purely excitonic states.<sup>35</sup> If the the cavity photon energy is resonant with the electronic transition, the energy difference between LP and UP at normal incidence is known as the Rabi splitting, which can be expressed as

$$\hbar\Omega_{R} = 2\sqrt{\sum_{i}(\hbar g_{i})^{2}} = 2\|\boldsymbol{\mu}\|\sqrt{\frac{\hbar\omega_{c}\sum_{i=1}^{N}\cos^{2}\theta_{i}}{2\epsilon_{0}\epsilon_{\infty}V}}$$
(2)

If these N excitons are randomly oriented, the average value of  $\cos^2\theta_i$  is

$$\overline{\cos^2\theta} = \frac{1}{4\pi} \int_0^{\pi} \cos^2\theta \sin\theta \, d\theta \int_0^{2\pi} d\varphi = \frac{1}{3}$$
 (3)

The Rabi splitting within such random orientation model becomes

$$\hbar\Omega_{\rm R} = \frac{2}{\sqrt{3}} \|\boldsymbol{\mu}\| \sqrt{\frac{\hbar\omega_{\rm c}N}{2\epsilon_0\epsilon_\infty V}} = \frac{2}{\sqrt{3}} \|\boldsymbol{\mu}\| \sqrt{\frac{\hbar\omega_{\rm c}\mathcal{C}}{2\epsilon_0\epsilon_\infty}}$$
(4)

where  $\mathcal{C}$  is the doping concentration of the light-emitting molecule in the matrix.

The LP state can be expressed as (following Tavis-Cummings model) $^3$ 

$$|\text{LP}\rangle = C_0|g;1\rangle + C_1|e_1^{S_1};0\rangle + C_2|e_2^{S_1};0\rangle + \dots + C_N|e_N^{S_1};0\rangle$$
 (5)

Note that 0 and 1 denote the photon states;  $|g;1\rangle$  represents the state with all molecules in the ground state and a cavity photon;  $|e_i^{S_1};0\rangle$  represents the state with the  $i^{th}$  molecule being excited and the cavity mode is in its ground state. The normalization condition reads

$$C_0^2 + \sum_{i=1}^N C_i^2 = 1 \tag{6}$$

The energy of LP is delocalized within N excitons and one cavity photon, and the value of  $C_0^2$  represents the photon contribution of LP. Practically,  $\{C_i\}$   $(i = 0, \dots, N)$  depends on the angle of incidence and the detuning value (the energy difference between the exciton absorption energy and the photon). For simplicity, we only consider the case at normal incidence.

Normally, the rISC process corresponds to the electronic transition from triplets to singlets promoted by SOC. According to Fermi's golden rule (FGR) and TVCF rate formalism, the rISC rate constant can be calculate as <sup>20,36</sup>

$$k_{\rm rISC} = \frac{1}{h^2} |H_{\rm if}^{\rm SO}|^2 \int_{-\infty}^{+\infty} dt e^{i\omega_{\rm if}t} \rho_{\rm fi}(t,T)$$
 (7)

where  $H_{\rm if}^{\rm SO}$ ,  $\omega_{\rm if}$ ,  $\rho_{\rm fi}(t,T)$  correspond to the SOC constant, the frequency difference, and the Frank-Condon overlap between the initial (triplet) and final (singlet) state. Within strong LMC regime, the rISC process may also take place between the triplet state and the LP state, of which the rate constant might be significantly altered. To compute the rISC rate constant from a triplet to LP, one first needs to notice that vibronic decoupling will occur if the Rabi frequency is larger than the highest frequency vibrational modes coupled to the exciton states.  $^{28,37,38}$  In such scenario, the geometric configuration of LP remains the same as that of the ground state. Therefore, the Frank-Condon overlap that enters the FGR rate equation would become the one between triplet and the ground state (instead of that between triplet and singlet excited states). As shown experimentally via the absorption and emission spectra in Ref. 15, such vibronic decoupling indeed takes place for ErB inside the cavity under strong LMC, i.e., the absorption and emission peaks are identical. If one takes the vibronic decoupling effect into account and considers SOC between  $T_1$  and the excitonic part of LP as the only promoting force, the rISC rate constant from triplet to LP (termed

as  $k_{\text{rISC},1}^{\text{T}_1 \to \text{LP}}$  here) becomes

$$k_{\text{rISC},1}^{\text{T}_1 \to \text{LP}} = \frac{1}{h^2} |H_{\text{if}}^{\text{SO}}|^2 \int_{-\infty}^{+\infty} dt e^{i[\omega_{\text{if}} - \frac{\Omega_{\text{R}}}{2}]t} \rho_{0\text{T}_1}(t,T) \times \frac{\sum_i C_i^2}{N_{\text{eff}}}$$
(8)

where  $\rho_{0T_1}(t,T)$  is the Frank-Condon overlap between the ground state and the  $T_1$  state and  $N_{\rm eff}$  corresponds to the effective number of molecules that couple to the field. Note that under random orientation assumption,  $N_{\rm eff}$  is around one third of the total molecule inside the cavity, as can be easily seen from Eqn. 4. The classical limit of Eqn. 8 is the Marcus equation for the rISC process from  $T_1$  to LP triggered by SOC, which has been proposed and extensively discussed in Refs. 27 and 28, and the mechanism of such SOC-triggered rISC process is schematically depicted in Figure 1(a).

While Eqn. 8 can be used to evaluate the polariton-enhanced rISC rate for most fluorescent molecules, what has been excluded is the transition from triplet to LP triggered by the coupling between the triplet state and the photonic part of LP, i.e., the coupling to the first term of Eqn. 5 from the triplet state. For molecules with phosphorescent phenomenon or non-negligible TDM of  $T_1$ , such coupling needs to be taken into consideration. If the TDM of  $T_1$  is  $\mu_{T_1}$ , then the collective LMC between N randomly oriented triplet excitons and the cavity mode can be written as

$$\hbar\Omega_{\mathrm{T}_{1}} = \frac{1}{\sqrt{3}} \|\boldsymbol{\mu}_{\mathrm{T}_{1}}\| \sqrt{\frac{\hbar\omega_{\mathrm{c}}N}{2\epsilon_{0}\epsilon_{\infty}V}} = \frac{1}{\sqrt{3}} \|\boldsymbol{\mu}_{\mathrm{T}_{1}}\| \sqrt{\frac{\hbar\omega_{\mathrm{c}}\mathcal{C}}{2\epsilon_{0}\epsilon_{\infty}}}$$
(9)

where  $\omega_c$ ,  $\mathcal{C}$ ,  $\epsilon_0$ ,  $\epsilon_\infty$  share the same definition as in Eqns. 2 and 4. Note that by coupling with the cavity mode, these triplets become coherent excitons and the collective LMC is enhanced by a factor of  $\sqrt{N_{\text{eff}}}$  (compared with the case of molecular excited triplets),<sup>2</sup> which equals  $\sqrt{N/3}$  with orientational average for randomly oriented excitons. A brief derivation of Eqn. 9 is given in Supporting Information. Owing to the fact that the TDM of the  $T_1$  state is usually much smaller than that of bright singlet state, even for phosphorescent molecules, the coupling strength between triplet and the cavity mode is usually within the weak coupling

regime, i.e., no hybrid polaritonic states will be formed between the triplet exciton and the photon. For molecules with non-negligible TDM of  $T_1$ , the rISC process triggered by the collective LMC between a set of coherent  $T_1$  states and the cavity mode (termed as  $k_{rISC,2}^{T_1 \to LP}$  here) can be expressed as

$$k_{\text{rISC},2}^{\text{T}_1 \to \text{LP}} = \frac{1}{h^2} |\hbar \Omega_{\text{T}_1}|^2 \int_{-\infty}^{+\infty} dt e^{i[\omega_{\text{if}} - \frac{\Omega_{\text{R}}}{2}]t} \rho_{0\text{T}_1}(t,T) \times C_0^2$$
 (10)

At resonance,  $C_0^2 = \sum_i C_i^2 = 0.5$ ,  $k_{\rm rISC,2}^{\rm T_1 \to LP}$  would become significant if the TDM of  $T_1$  is not negligible, and efficient rISC can then be initiated if the population on triplet state after excitation is sufficient, which can be achieved via either a significantly faster ISC rate from  $S_1$  to  $T_1$  compared to the radiative/nonradiative decay rate of  $S_1/T_1$  and the rISC rate from  $T_1$  to  $S_1$  under photo-excitation, or the direct formation under current injection. The mechanism of the LMC-promoted rISC process from coherent  $T_1$  to LP is schematically depicted in Figure 1(b).

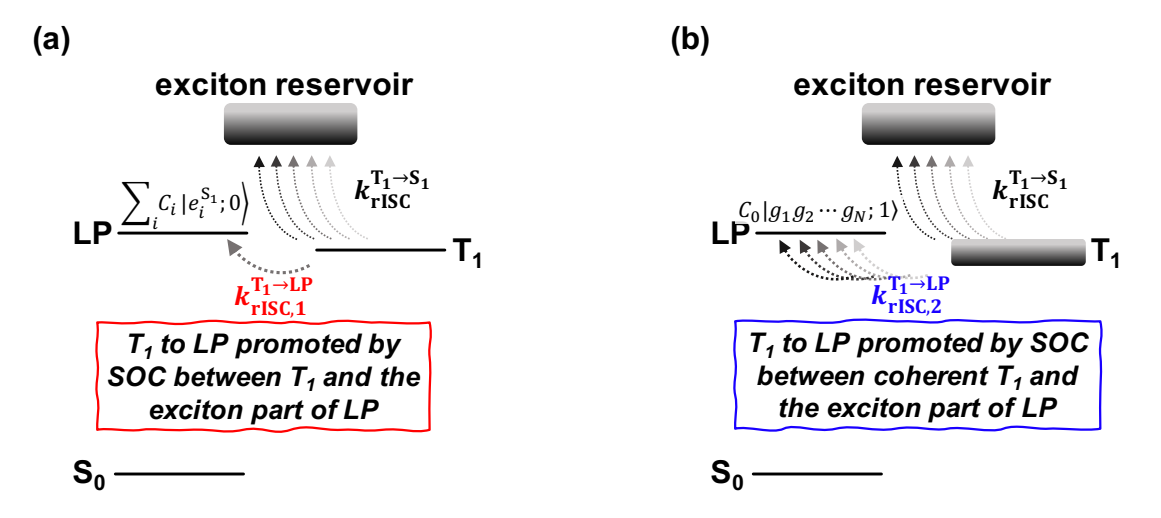


Figure 1: Schematic graph of two possible rISC channels. (a)  $T_1$  to LP rISC process promoted by the SOC between  $T_1$  and the exciton part of LP, with the corresponding rate constant  $k_{\text{rISC},1}^{T_1 \to \text{LP}}$ . (b)  $T_1$  to LP rISC process promoted by the collective LMC between coherent  $T_1$  and the photonic part of LP, with the corresponding rate constant  $k_{\text{rISC},2}^{T_1 \to \text{LP}}$ .

#### Results and Discussion

#### Outside the cavity: electronic structure and transitions of ErB

The geometries of the  $S_0$ ,  $S_1$ , and  $T_1$  states of isolated ErB molecule are first optimized via density functional theory (DFT) and time-dependent DFT (TDDFT) with B3LYP functional and def2-svp basis set with corresponding def2 effective core potential (ECP). The excitation energies are then evaluated via spin-flip TDDFT (SF-TDDFT)<sup>39,40</sup> with B3LYP funtional and def2-svpd basis set with corresponding ECP, since TDDFT gives severely deviant predictions of the absorption energy of  $S_1$  and the emission energy of  $T_1$  as shown in Table S1. It can be seen in Table 1 that the excitation energies computed via SF-TDDFT/B3LYP are in line with the experimental values. Two suggested functionals from previous study, B5050LYP and PBE50,<sup>41</sup> are tested for SF-TDDFT calculation, and resultant energies are not as satisfying as those from B3LYP (as shown in Table S1). Explicit values of the TDM of  $S_1/T_1$  and the SOC between  $S_0/S_1$  and  $T_1$  for ErB, as well as the computational details are given in Methods and Supporting Information.

With the electronic structure information, we calculate the rate constants of various electronic transition via TVCF rate formalism. Calculated results are listed in Table 1, together with the corresponding experimental values for comparison. An excellent agreement can be found between the theoretical predicted rate constants and their experimental counterparts, which rationalizes our applied electronic structure methods and TVCF rate formalism. Note that the ISC rate constant of ErB is significantly larger than the radiative/nonradiative decay rate of  $S_1$  and  $T_1$  as well as the rISC rate, which leads to asufficient population on the  $T_1$  state after excitation, and can thus contribute to the presumable enhancement of the rISC process inside the cavity.

Table 1: Absorption/emission energies of  $S_1$  and  $T_1$ , the 0-0 singlet-triplet energy gap  $\Delta E_{ST}^{00}$ , as well as various rate constants of ErB predicted by SF-TDDFT/B3LYP/def2-svpd (with corresponding ECP) and TVCF rate formalism. Experimental results are also listed for comparison.

Energetics	Exp. $(eV)^a$	Cal. (eV)
$\overline{S_1}$ absorption	2.305	2.448
$S_1$ emission	2.234	2.145
$T_1$ emission	1.845	1.893
$\Delta E_{ m ST}^{00}$	0.426	0.386
Rate constants <sup><math>b</math></sup>	Exp. $(s^{-1})^c$	Cal. $(s^{-1})$
$k_{ m F}$	$2.8 \times 10^{8}$	$1.5 \times 10^{8}$
$k_{ m nr,S_1}$	$1.6 \times 10^{8}$	$0.76 \times 10^{8}$
$k_{ m ISC}$	$1.1 \times 10^9$	$0.88 \times 10^9$
$k_{ m rISC}$	$5.1 \times 10^{1}$	$7.1 \times 10^{1}$
$k_{ m P}$	$4.1 \times 10^{1}$	$9.3 \times 10^{1}$
$k_{ m nr,T_1}$	$1.5 \times 10^{3}$	$1.3 \times 10^{3}$

<sup>&</sup>lt;sup>a</sup>Experimental energetics are obtained from Ref. 15;

 $<sup>{}^</sup>bk_{\rm F},\,k_{\rm nr,S_1},\,k_{\rm ISC},\,k_{\rm rISC},\,k_{\rm P},\,$  and  $k_{\rm nr,T_1}$  correspond to the fluorescent radiative decay rate of  $S_1$ , the nonradiative decay rate from  $S_1$  to  $S_0$ , the ISC rate from  $S_1$  to  $T_1$ , the rISC rate from  $T_1$  to  $S_1$ , the phosphorescent radiative decay rate of  $T_1$ , and the nonradiative decay rate from  $T_1$  to  $S_0$ , respectively;

<sup>&</sup>lt;sup>c</sup>Experimental rate constants are obtained from Ref. 42

#### Inside the cavity: light-matter coupling and enhanced rISC

The next step is to calculate the LMC of ErB and the cavity mode at different doping concentrations (within the strong coupling regime) based on the experiments,  $^{15}$  0.27 M, 0.36 M, 0.45 M, 0.54 M, and 0.61 M. It should be noted that ErB is a phosphorescent molecule with non-negligible TDM of  $T_1$ . Therefore, we compute the coupling to the cavity mode from both  $S_1$  and  $T_1$  exciton from Eqn. 4 and Eqn. 9, respectively. The optical dielectric constant  $\epsilon_{\infty}$  of PVA is calculated as the square of its refractive index n=1.53, i.e.,  $\epsilon_{\infty}=n^2=2.34.^{43,44}$  It can be seen from Table 2 that the coupling between  $S_1$  and the cavity mode is large enough for all investigated doping concentrations, and two polaritonic bands can therefore be formed inside the cavity, which is consistent with the experimental absorption spectra. Specifically, when  $\mathcal{C}$  is 0.54 M, the computed Rabi splitting is 413 meV, and corresponding excitation energy of LP is 2.241 eV, which are in good agreement with the experimentally measured values (375 meV and 2.187 eV). <sup>15</sup> The coupling from T<sub>1</sub> to the cavity mode is much smaller compared to that from S<sub>1</sub>, and therefore T<sub>1</sub> is unlikely to be hybridized with the photonic component for all doping concentrations, which is again consistent with the experimental findings that the phosphorescence spectra of the system basically remain the same with or without the cavity. <sup>15</sup> However, such coupling may become the additional promoting force (other than SOC) that triggers off the rISC process from T<sub>1</sub> to LP.

Table 2: LMC between  $S_1/T_1$  exciton of ErB and the cavity mode, the corresponding excitation energy of LP and 0-0 LP-triplet energy gap at different doping concentrations.

$\mathcal{C}(M)$	$\hbar\Omega_{\rm R}~({\rm eV})$	$\hbar\Omega_{\rm T_1}~({\rm cm}^{-1})$	$E_{\rm LP}~({\rm eV})^a$	$\Delta E_{\text{LP,T}_1}^{00} \text{ (eV)}$
0.27	0.292	1.184	2.302 (2.223)	0.339
0.36	0.338	1.367	2.279(2.214)	0.316
0.45	0.377	1.528	2.259(2.194)	0.301
0.54	0.413	1.674	2.241(2.187)	0.283
0.61	0.439	1.780	2.228	0.270

<sup>&</sup>lt;sup>a</sup>In the parentheses are experimental data obtained from Ref. 15 (which corresponds to the emission energies of LP at various doping concentrations).

While it is nontrivial to evaluate the exact number of excitons that couple to the cavity mode due to the lack of some experimental details such as the cavity photon density, we assume the width and length of the cavity is two times the value of the experimentally measured thickness of the doped film, i.e., 130 nm, and evaluate the total number of emitters inside the cavity via

$$N = \mathcal{C}VN_{\rm A} \tag{11}$$

where  $N_{\rm A}$  is the Avogadro constant. For  $\mathcal{C}=0.54$  M, N is  $2.8\times 10^6$  based on Eqn. 11, and the number of effectively coupled excitons  $N_{\rm eff}$  is around  $10^5$  to  $10^6$  for randomly oriented molecules, which is of the similar order as estimated in Ref. 28. If  $N_{\rm eff}=10^5$  (at  $\mathcal{C}=0.54$  M), the resulting  $k_{\rm rISC,1}^{\rm T_1\to LP}$  evaluated from Eqn. 8 will be less than  $1~{\rm s}^{-1}$  with a resonant condition as applied in the experiment ( $\sum_i C_i^2 = C_0^2 = 0.5$ ). The experimentally observed enhancement of the  $T_1$  decay rate is with the order of  $10^3$ , which is significantly larger than the estimated value of  $k_{\rm rISC,1}^{\rm T_1\to LP}$ , i.e., the enhancement of rISC of ErB inside the cavity cannot be rationally described via Eqn. 8.

We now evaluate the enhanced rISC process from the other promoting force, i.e., the collective LMC between coherent  $T_1$  and the cavity mode, and such enhancement corresponds to  $k_{\text{rISC},2}^{\text{T1}\to\text{LP}}$ , which can be directly calculated via TVCF rate formalism (as shown in Eqn. 10) with the LMC given by Eqn. 9. According to Ref. 15, the experimental rISC rate constant can be obtained by taking the reciprocal of the  $T_1$  lifetime and subtracting the radiative and nonradiative decay rate constants of  $T_1$  back to  $S_0$ , namely,  $k_P$  and  $k_{\text{nr},T_1}$ . Nevertheless, special attention needs to be paid here, as the decay processes of  $T_1$  might be influenced by some nontrivial aggregation-induced effect when the doping concentration increases, which is irrelevant to the cavity-enhanced rISC. To make a reasonable comparison with the experimental data and rule out such aggregation-induced effect, we define the experimental cavity-promoted enhancement of the rISC rate constant as the difference between the total decay rate of  $T_1$  inside the cavity and that outside the cavity. Both the theoretical  $k_{\text{rISC},2}^{T_1\to\text{LP}}$  and the experimental enhancement are plotted in Figure 2 with respect to various doping

concentrations. Explicit values of theoretical  $k_{\mathrm{rISC,2}}^{\mathrm{T_1 \to LP}}$  and experimental enhanced rISC rate for different doping concentrations are listed in Table S3. It can be seen from Figure 2 that the theoretically predicted enhancement given by Eqn. 10 is in a good agreement with the experimentally observed enhancement for all tested doping concentrations, which evinces the fact that the LMC between  $\mathrm{T_1}$  and the cavity mode does act as an alternative promoting force and enhance the rISC process. With the increase of the doping concentration, the energy barrier of the rISC process is decreased and the coupling between  $\mathrm{T_1}$  and the cavity mode is increased, leading to a continuously enhanced rISC from  $\mathrm{T_1}$  to LP. We also investigate the individual effect of the reduced energy barrier and the increased LMC between  $\mathrm{T_1}$  and the field to the overall enhancement of the rISC process inside the cavity as shown in Figure S2. Note that even though the total enhancement of  $k_{\mathrm{rISC,2}}^{\mathrm{T_1 \to LP}}$  mainly stems from the reduced energy barrier as the doping concentration increases, the LMC between  $\mathrm{T_1}$  and LP is the essential precondition that initiates such rISC process.

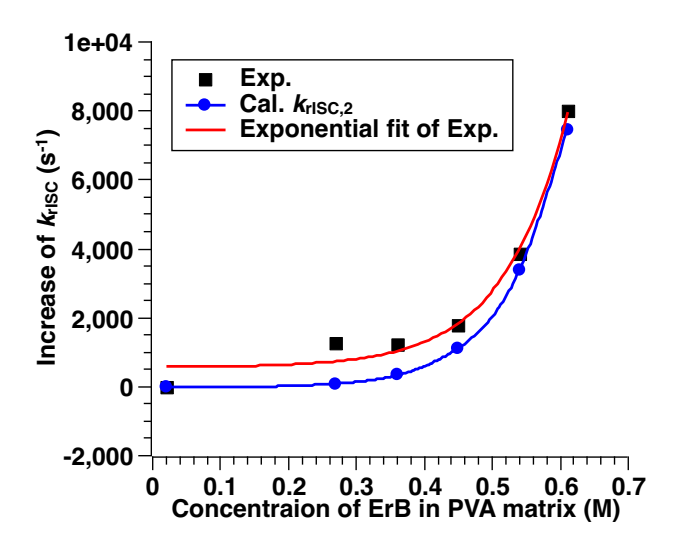


Figure 2: Experimental (black square) and calculated (blue circle) polaritonic enhancement to the rISC process of ErB with respect to different doping concentrations. The red line corresponds to an exponential fit based on the experimental data from Ref. 15.

Next, we consider the temperature effects to the enhanced rISC process. The rISC process of ErB is a thermally activated process and thus very sensitive to the change of temperature. Experimentally, the increase of rISC rate constant with respect to the increase

of the temperature has been observed inside the cavity within a wide temperature range (from 283 K to 333 K) for C = 0.54 M. Theoretically, we calculate  $k_{\rm rISC,2}^{\rm T_1 \to LP}$  at different temperatures with the rISC energy barrier and coupling strength obtained from C = 0.54 M and the results are shown in Figure 3, together with the experimentally observed rISC enhancement at different temperatures for comparison. Explicit values are listed in Table S4. As shown in Figure 3, the theoretical predicted enhancement of rISC process qualitatively matches with the experimental results within the tested temperature range. A more rapid growth with respect to the temperature is found in the theoretical results, which may correspond to a slightly overestimated energy barrier according to Arrhenius law. Such discrepancy may also arise from the fact that the optical dielectric constant of PVA marginally changes as temperature increases. The overall tendency of the rISC enhancement inside the cavity, however, can be qualitatively reproduced via the theoretically computed  $k_{\text{rISC},2}^{\text{T}_1 \to \text{LP}}$ , and such agreement further justifies the rationality of the LMC between  $T_1$  and the cavity mode acting as an effective promoting force that enhances the rISC process for ErB. The temperature dependence of  $k_{\mathrm{rISC},1}^{\mathrm{T}_1 \to \mathrm{LP}}$  has also been investigated in Figure S3. As shown in Figure S3, despite the fact that  $k_{\text{rISC},1}^{\text{T}_1 \to \text{LP}}$  given by Eqn. 8 has a remarkable temperature dependence, its contribution to the overall enhancement would still be negligible even at high temperatures, due to the large number of molecules that effectively couple to the cavity.

As we have shown above, by taking the collective LMC between  $T_1$  and the cavity mode into account, we are able to reproduce the experimentally observed enhancement to the rISC rate of ErB inside the cavity via TVCF rate formalism. Note that this enhanced rISC channel might be safely ignored for fluorescent molecules with negligible TDM of  $T_1$ . For example, the molecule that has been investigated in Ref. 28, 3DPA3CN, is a TADF molecule with almost no phosphorescence even at low temperature, <sup>45</sup> which corresponds to an infinitesimal LMC between  $T_1$  and the cavity mode. Therefore, the rISC of 3DPA3CN inside the cavity is not noticeably enhanced via  $k_{\text{rISC},2}^{T_1 \to \text{LP}}$ . In addition to the TDM of  $T_1$ , another key factor to obtain considerable enhancement of the rISC via the LMC between  $T_1$  and the field is

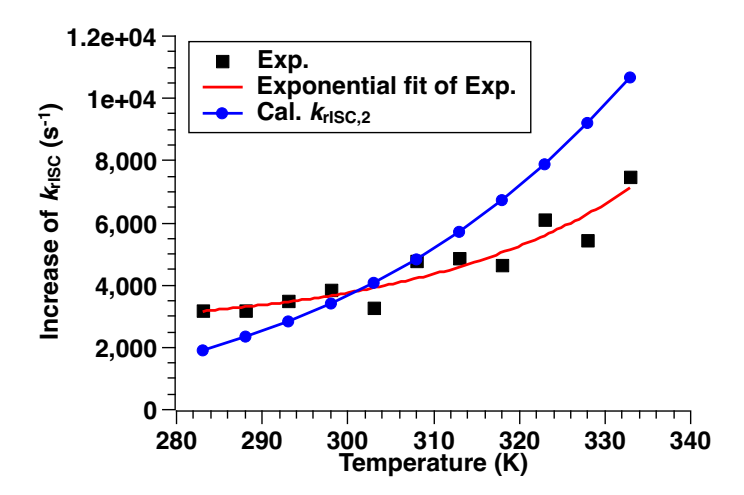


Figure 3: Experimental (black square) and calculated (blue circle) polaritonic enhancement to the rISC process of ErB with respect to different temperatures. The red line corresponds to an exponential fit based on the experimental enhancement computed via the data from Ref. 15.

that  $T_1$  possesses a substantial population after the excitation, which may be introduced via either the direct formation of triplets under current injection or a significantly faster ISC rate compared to the radiative and nonradiative decay rate of  $S_1$  and  $T_1$  under photo-excitation. It should be noted that even the tested system here (ErB) is a phosphorescent molecule, such enhancement via  $k_{\text{rISC},2}^{T_1 \to \text{LP}}$  can be expected for normal TADF emitters as long as the  $T_1$  state of these emitters has a sizable ISC-induced TDM.

## Conclusion

In summary, we have unravelled an alternative promoting force, in addition to the SOC between  $T_1$  and LP, for the polariton-enhanced rISC process inside the cavity, i.e., the collective LMC between coherent  $T_1$  states and the cavity mode that initiates the conversion from  $T_1$  to LP without perturbing the energy level of the original  $T_1$  state. This promoting force is necessary to be taken into account for molecules with a non-negligible TDM of  $T_1$ . With this revised mechanism, we are able to reproduce the experimentally observed polariton-enhanced rISC rate constant of ErB inside a caivty, and demonstrate that the

enhanced rISC of ErB inside the cavity can be effectively promoted by the LMC between its  $T_1$  and the cavity mode. While the effect of the LMC between  $T_1$  and LP to the rISC process has rarely been investigated in previous studies, what we have concluded here is that such coupling makes it possible for poor or even non-TADF emitters to harvest triplet exciton for fluorescence inside a cavity, as long as these emitters have a sizable TDM of  $T_1$ . Such findings will substantially widen the aperture of TADF candidates. Looking forward, we believe this theoretical protocol would immediately benefit the illumination of important experimental phenomena as well as the design of polariton-enhanced TADF systems.

#### Methods

All of the electronic structure calculations are carried out using quantum chemistry package Q-CHEM 5.3<sup>46</sup> except for the TDM calculation of T<sub>1</sub>, which is performed using DALTON. <sup>47</sup> All of the rate constant calculations are performed in our self-developed molecular material property prediction package MOMAP 2021A. <sup>48–50</sup> The SOC constants between singlet and triplet (constructed from TDDFT/B3LYP) of ErB are evaluated in a local developed version of Q-CHEM via the Breit-Pauli Hamiltonian <sup>51</sup> (one-electron part only) with the effective nuclear charge (ENC) obtained from Ref. 52 for C, H, O, Na and from Ref. 53 for I. All elements are tackled with all-electron basis set for the calculation of SOC and the TDM of T<sub>1</sub>, i.e., 6-311G\*\* for I and def2-svpd for C, H, O, and Na, and the values of ENC obtained from literature correspond to those used for all-electron basis set. The TDM of S<sub>1</sub> is calculated via SF-TDDFT/B3LYP/def2-svpd (with corresponding def2 ECP), while that of T<sub>1</sub> is calculated via the quadratic response method. <sup>54</sup> Additional computational details can be found in Supporting Information.

## Acknowledgement

QO thanks Dr. Wenjie Dou and Dr. Jiajun Ren for helpful discussion on the light-matter coupling between triplet and the cavity mode. ZS acknowledges financial support from the National Natural Science Foundation of China (Grant No. 21788102) as well as the Ministry of Science and Technology of China through the National Key R&D Plan (Grant No. 2017YFA0204501). YS is supported by the National Science Foundation (Grant No. CHE-2102071). QO acknowledges financial support from the National Natural Science Foundation of China (Grant No. 22003030), China Postdoctoral Science Foundation (Grant No. 2020M670280), and the Shuimu Tsinghua Scholar Program.

## Supporting Information Available

The Supporting Information is available free of charge on the ACS Publications website: Excitation energies of  $S_1$  and  $T_1$  of ErB predicted by TDDFT/B3LYP/def2-svpd. TDM of  $S_1$  and  $T_1$  of ErB, SOC between  $S_0/S_1$  and  $T_1$  of ErB, explicit rate constants of theoretically predicted  $k_{\text{rISC},2}^{T_1 \to \text{LP}}$  and experimentally observed rISC enhancement, the individual effect of the reduced energy barrier and the increased LMC strength to the overall  $k_{\text{rISC},2}^{T_1 \to \text{LP}}$ , temperature dependence of estimated  $k_{\text{rISC},1}^{T_1 \to \text{LP}}$  for  $\mathcal{C} = 0.54$  M, and additional computational details.

### References

- (1) Keeling, J.; Kéna-Cohen, S. Bose-Einstein Condensation of Exciton-Polaritons in Organic Microcavities. *Annu. Rev. Phys. Chem.* **2020**, *71*, 435–459.
- (2) Hertzog, M.; Wang, M.; Mony, J.; Börjesson, K. Strong Light-Matter Interactions: A New Direction within Chemistry. Chem. Soc. Rev. 2019, 48, 937–961.

- (3) Ribeiro, R. F.; Martínez-Martínez, L. A.; Du, M.; Campos-Gonzalez-Angulo, J.; Yuen-Zhou, J. Polariton Chemistry: Controlling Molecular Dynamics with Optical Cavities. Chem. Sci. 2018, 9, 6325–6339.
- (4) Ebbesen, T. W. Hybrid Light–Matter States in a Molecular and Material Science Perspective. Acc. Chem. Res. 2016, 49, 2403–2412.
- (5) Dovzhenko, D. S.; Ryabchuk, S. V.; Rakovich, Y. P.; Nabiev, I. R. Light-Matter Interaction in the Strong Coupling Regime: Configurations, Conditions, and Applications. *Nanoscale* 2018, 10, 3589–3605.
- (6) Schwartz, T.; Hutchison, J. A.; Genet, C.; Ebbesen, T. W. Reversible Switching of Ultrastrong Light-Molecule Coupling. *Phys. Rev. Lett.* **2011**, *106*, 196405.
- (7) Hutchison, J. A.; Schwartz, T.; Genet, C.; Devaux, E.; Ebbesen, T. W. Modifying Chemical Landscapes by Coupling to Vacuum Fields. Angew. Chem. Int. Ed. 2012, 51, 1592–1596.
- (8) Galego, J.; Garcia-Vidal, F. J.; Feist, J. Many-Molecule Reaction Triggered by a Single Photon in Polaritonic Chemistry. *Phys. Rev. Lett.* **2017**, *119*, 136001.
- (9) Munkhbat, B.; Wersäll, M.; Baranov, D. G.; Antosiewicz, T. J.; Shegai, T. Suppression of Photo-Oxidation of Organic Chromophores by Strong Coupling to Plasmonic Nanoantennas. *Sci. Adv.* **2018**, *4*, eaas9552.
- (10) Coles, D. M.; Niccolo Somaschi, P. M.; Clark, C.; Lagoudakis, P. G.; Savvidis, P. G.; Lidzey, D. G. Polariton-Mediated Energy Transfer between Organic Dyes in a Strongly Coupled Optical Microcavity. *Nat. Mater.* 2014, 13, 712–719.
- (11) Zhong, X.; Chervy, T.; Wang, S.; George, J.; Thomas, A.; Hutchison, J. A.; Devaux, E.; Genet, C.; Ebbesen, T. W. Non-Radiative Energy Transfer Mediated by Hybrid Light-Matter States. Angew. Chem. Int. Ed. 2016, 55, 6202–6206.

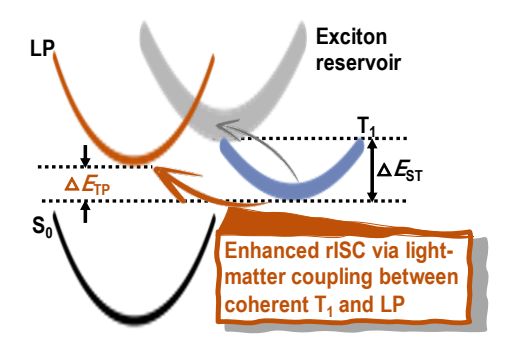
- (12) Zhong, X.; Chervy, T.; Zhang, L.; Thomas, A.; George, J.; Genet, C.; Hutchison, J. A.; Ebbesen, T. W. Energy Transfer between Spatially Separated Entangled Molecules. Angew. Chem. Int. Ed. 2017, 56, 9034–9038.
- (13) Georgiou, K.; Michetti, P.; Gai, L.; Cavazzini, M.; Shen, Z.; Lidzey, D. G. Control over Energy Transfer between Fluorescent BODIPY Dyes in a Strongly Coupled Microcavity. ACS Photonics 2018, 5, 258–266.
- (14) Kéna-Cohen, S.; Forrest, S. R. Green Polariton Photoluminescence Using the Red-Emitting Phosphor PtOEP. *Phys. Rev. B* **2007**, *76*, 075202.
- (15) Stranius, K.; Hertzog, M.; Börjesson, K. Selective Manipulation of Electronically Excited States through Strong Light–Matter Interactions. *Nat. Commun.* **2018**, *9*, 2273.
- (16) Kéna-Cohen, S.; Forrest, S. R. Room-temperature polariton lasing in an organic single-crystal microcavity. *Nat. Photonics* **2010**, *4*, 371–375.
- (17) Bittner, E. R.; Silva, C. Estimating the Conditions for Polariton Condensation in Organic Thin-Film Microcavities. *J. Chem. Phys.* **2012**, *136*, 034510.
- (18) Daskalakis, K. S.; Maier, S. A.; Murray, R.; Kéna-Cohen, S. Nonlinear Interactions in An Organic Polariton Condensate. *Nat. Mater.* **2014**, *13*, 271–278.
- (19) Paschos, G. G.; Somaschi, N.; Tsintzos, S. I.; Coles, D.; Bricks, J. L.; Hatzopoulos, Z.; Lidzey, D. G.; Lagoudakis, P. G.; Savvidist, P. G. Hybrid Organic-Inorganic Polariton Laser. Sci. Rep. 2017, 7, 11377.
- (20) Peng, Q.; Fan, D.; Duan, R.; Yi, Y.; Niu, Y.; Wang, D.; Shuai, Z. Theoretical Study of Conversion and Decay Processes of Excited Triplet and Singlet States in a Thermally Activated Delayed Fluorescence Molecule. J. Phys. Chem. C 2017, 121, 13448–13456.
- (21) Xu, S.; Yang, Q.; Wan, Y.; Chen, R.; Wang, S.; Si, Y.; Yang, B.; Liu, D.; Zheng, C.; Huang, W. Predicting Intersystem Crossing Efficiencies of Organic Molecules for Effi-

- cient Thermally Activated Delayed Fluorescence. J. Mater. Chem. C 2019, 7, 9523–9530.
- (22) Cui, L.-S.; Gillett, A. J.; Zhang, S.-F.; Ye, H.; Liu, Y.; Chen, X.-K.; Lin, Z.-S.; Evans, E. W.; Myers, W. K.; Ronson, T. K.; Nakanotani, H.; Reineke, S.; Bredas, J.-L.; Adachi, C.; Friend, R. H. Fast Spin-Flip Enables Efficient and Stable Organic Electro-luminescence from Charge-Transfer States. Nat. Photonics 2020, 14, 636–642.
- (23) Zhan, X.; Wu, Z.; Gong, Y.; Tu, J.; Xie, Y.; Peng, Q.; Ma, D.; Li, Q.; ; Li, Z. Utilizing Electroplex Emission to Achieve External Quantum Efficiency up to 18.1% in Nondoped Blue OLED. *Research* **2020**, *2020*, 8649102.
- (24) Xu, J.; Tang, X.; Zhao, X.; Zhu, H.; Qu, F.; Xiong, Z. Abnormal Reverse Intersystem Crossing of Polaron-Pair States and Its Conversion to Intersystem Crossing via the Regulation of Intermolecular Electron-Hole Spacing Distance. *Phys. Rev. Appl.* 2020, 14, 024011.
- (25) Polak, D. et al. Manipulating Molecules with Strong Coupling: Harvesting Triplet Excitons in Organic Exciton Microcavities. *Chem. Sci.* **2020**, *11*, 343–354.
- (26) Yu, Y.; Mallick, S.; Wang, M.; Börjesson, K. Barrier-Free Reverse-Intersystem Crossing in Organic Molecules by Strong Light-Matter Coupling. *Nat. Commun.* **2021**, *12*, 3255.
- (27) Martínez-Martínez, L. A.; Eizner, E.; Kéna-Cohen, S.; Yuen-Zhou, J. Triplet Harvesting in the Polaritonic Regime: A Variational Polaron Approach. J. Chem. Phys. 2019, 151, 054106.
- (28) Eizner, E.; Martínez-Martínez, L. A.; Yuen-Zhou, J.; Kéna-Cohen, S. Inverting Singlet and Triplet Excited States Using Strong Light-Matter Coupling. *Sci. Adv.* **2019**, *5*, eaax4482.

- (29) Koch, A.; Kinzel, D.; Dröge, F.; Gräfe, S.; Kupfer, S. Photochemistry and Electron Transfer Kinetics in a Photocatalyst Model Assessed by Marcus Theory and Quantum Dynamics. J. Phys. Chem. C 2017, 121, 16066–16078.
- (30) Menger, M. F. S. J.; Plasser, F.; Mennucci, B.; González, L. Surface Hopping within an Exciton Picture. An Electrostatic Embedding Scheme. J. Chem. Theory Comput. 2018, 14, 6139–6148.
- (31) Westermayr, J.; Gastegger, M.; Menger, M. F. S. J.; Mai, S.; González, L.; Marquetand, P. Machine Learning Enables Long Time Scale Molecular Photodynamics Simulations. Chem. Sci. 2019, 10, 8100–8107.
- (32) Shuai, Z.; Peng, Q. Excited States Structure and Processes: Understanding Organic Light-Emitting Diodes at the Molecular Level. *Physics Reports* **2014**, *537*, 123–156.
- (33) Wang, Y.; Peng, Q.; Ou, Q.; Lin, S.; Shuai, Z. A Novel Molecular Descriptor for Highly Efficient (Φ<sub>TADF</sub> > 90%) Transition Metal TADF Au(iii) Complexes. J. Mater. Chem. A 2020, 8, 18721–18725.
- (34) Lin, S.; Ou, Q.; Wang, Y.; Peng, Q.; Shuai, Z. Aggregation-Enhanced Thermally Activated Delayed Fluorescence Efficiency for Two-Coordinate Carbene–Metal–Amide Complexes: A QM/MM Study. J. Phys. Chem. Lett. 2021, 12, 2944–2953.
- (35) Houdré, R.; Stanley, R. P.; Ilegems, M. Vacuum-Field Rabi Splitting in the Presence of Inhomogeneous Broadening: Resolution of a Homogeneous Linewidth in an Inhomogeneously Broadened System. Phys. Rev. A 1996, 53, 2711–2715.
- (36) Niu, Y.; Peng, Q.; Deng, C.; Gao, X.; Shuai, Z. Theory of Excited State Decays and Optical Spectra: Application to Polyatomic Molecules. *J. Phys. Chem. A* **2010**, *114*, 7817–7831.

- (37) Spano, F. C. Optical Microcavities Enhance the Exciton Coherence Length and Eliminate Vibronic Coupling in J-Aggregates. *J. Chem. Phys.* **2015**, *142*, 184707.
- (38) Herrera, F.; Spano, F. C. Cavity-Controlled Chemistry in Molecular Ensembles. *Phys. Rev. Lett.* **2016**, *116*, 238301.
- (39) Shao, Y.; Head-Gordon, M.; Krylov, A. I. The Spin–Flip Approach within Time–Dependent Density Functional Theory: Theory and Applications to Diradicals. *J. Chem. Phys.* **2003**, *118*, 4807–4818.
- (40) Bernard, Y. A.; Shao, Y.; Krylov, A. I. General Formulation of Spin-Flip Time-Dependent Density Functional Theory Using Non-Collinear Kernels: Theory, Implementation, and Benchmarks. J. Chem. Phys. 2012, 136, 204103.
- (41) Orms, N.; Krylov, A. I. Singlet–Triplet Energy Gaps and the Degree of Diradical Character in Binuclear Copper Molecular Magnets Characterized by Spin-Flip Density Functional Theory. *Phys. Chem. Chem. Phys.* **2018**, *20*, 13127–13144.
- (42) Lettinga, M. P.; Zuilhof, H.; van Zandvoort, M. A. M. J. Phosphorescence and Fluorescence Characterization of Fluorescein Derivatives Immobilized in Various Polymer Matrices. *Phys. Chem. Chem. Phys.* 2000, 2, 3697–3707.
- (43) Matsumoto, S.; Ishii, T.; Wada, M.; Kuwahara, Y.; Ogata, T.; Nagaoka, S.; Takafuji, M.; Ihara, H. Facile Preparation of High Refractive Index Polymer Films Composited with a Tungstophosphoric Acid. *Mater. Lett.* 2017, 190, 236–239.
- (44) Robertson, J. In *Comprehensive Semiconductor Science and Technology*; Bhattacharya, P., Fornari, R., Kamimura, H., Eds.; Elsevier: Amsterdam, 2011; pp 132–176.
- (45) Taneda, M.; Shizu, K.; Tanaka, H.; Adachi, C. High Efficiency Thermally Activated Delayed Fluorescence Based on 1,3,5-tris(4-(diphenylamino)phenyl)-2,4,6-tricyanobenzene. *Chem. Commun.* **2015**, *51*, 5028–5031.

- (46) Shao, Y. et al. Advances in Molecular Quantum Chemistry Contained in the Q-Chem 4 Program Package. *Mol. Phys.* **2015**, *113*, 184–215.
- (47) Aidas, K. et al. The Dalton Quantum Chemistry Program System. WIREs Comput. Mol. Sci. 2014, 4, 269–284.
- (48) Shuai, Z.; Peng, Q. Organic Light-Emitting Diodes: Theoretical Understanding of Highly Efficient Materials and Development of Computational Methodology. Nat. Sci. Rev. 2017, 4, 224–239.
- (49) Peng, Q.; Yi, Y.; Shuai, Z.; Shao, J. Toward Quantitative Prediction of Molecular Fluorescence Quantum Efficiency: Role of Duschinsky Rotation. J. Am. Chem. Soc. 2007, 129, 9333–9339.
- (50) Shuai, Z. Thermal Vibration Correlation Function Formalism for Molecular Excited State Decay Rates. *Chin. J. Chem. 38*, 1223–1232.
- (51) Abegg, P. Ab Initio Calculation of Spin-Orbit Coupling Constants for Gaussian Lobe and Gaussian-Type Wave Functions. *Mol. Phys.* **1975**, *30*, 579–596.
- (52) Fedorov, D. G.; Koseki, S.; Schmidt, M. W.; Gordon, M. S. Spin-Orbit Coupling in Molecules: Chemistry beyond the Adiabatic Approximation. Int. Rev. Phys. Chem. 2003, 22, 551–592.
- (53) Chiodo, S. G.; Russo, N. One-Electron Spin-Orbit Contribution by Effective Nuclear Charges. J. Comput. Chem. 2009, 30, 832–839.
- (54) Vahtras, O.; Ågren, H.; Jørgensen, P.; Jensen, H. J. A.; Helgaker, T.; Olsen, J. Multiconfigurational Quadratic Response Functions for Singlet and Triplet Perturbations: The Phosphorescence Lifetime of Formaldehyde. J. Chem. Phys. 1992, 97, 9178–9187.



TOC Graphic